

UltimateDO: An Efficient Framework to Marry Occupancy Prediction with 3D Object Detection via Channel2height

Zichen Yu¹ Changyong Shu²✉

¹Dalian University of Technology, ²Houmo AI

yzichen@mail.dlut.edu.cn changyong.shu@houmo.ai

Abstract

Occupancy and 3D object detection are characterized as two standard tasks in modern autonomous driving system. In order to deploy them on a series of edge chips with better precision and time-consuming trade-off, contemporary approaches either deploy standalone models for individual tasks, or design a multi-task paradigm with separate heads. However, they might suffer from deployment difficulties (i.e., 3D convolution, transformer and so on) or deficiencies in task coordination. Instead, we argue that a favorable framework should be devised in pursuit of ease deployment on diverse chips and high precision with little time-consuming. Oriented at this, we revisit the paradigm for interaction between 3D object detection and occupancy prediction, reformulate the model with 2D convolution and prioritize the tasks such that each contributes to other. Thus, we propose a method to achieve fast 3D object detection and occupancy prediction (UltimateDO), wherein the light occupancy prediction head in FlashOcc is married to 3D object detection network, with negligible additional time-consuming of only 1.1ms while facilitating each other. We instantiate UltimateDO on the challenging nuScenes-series benchmarks.

1. Introduction

Holistic perception, encompassing both object-level and voxel-level representations, plays a crucial role in autonomous driving. In particular, the acquisition of 3D object bounding boxes and accurate occupancy predictions has gained significant traction among scholars and industry professionals alike, owing to their fundamental significance in ensuring the safety and dependability of autonomous vehicles. Early studies have traditionally employed separate networks to model object-level and voxel-level understanding. While this divide-and-conquer strategy simplifies algorithm development [7, 14, 16, 20, 22, 24, 25, 27, 28], it comes at the expense of sacrificing the jointly optimized enhancement for each task.

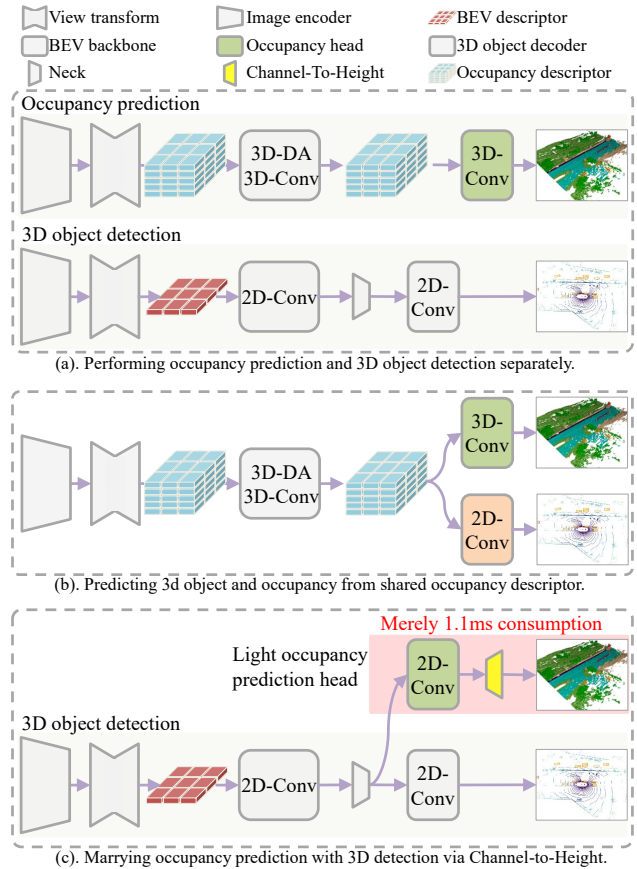


Figure 1. **Different paradigm of interaction between 3D object detection and occupancy prediction.** (a) performs occupancy prediction and 3D object detection separately. (b) shows the synchronous perception for detection and occupancy from shared voxel-level occupancy descriptor. (c) exhibits our UltimateDO where a light grafting occupancy module is married to 3D object detection. The abbreviation "Conv" represents convolution, "DA" denotes deformable convolution. Besides, the presence of "3D-DA", "3D-Conv" or "2D-Conv" in the icon indicates that the corresponding module is composed of these operators. Best viewed in color.

With the emergence of the end-to-end unified solution for autonomous driving system [6], an increasing number of studies have attempted to jointly integrate occupancy and detection within the same model. [13, 15] inject the occupancy knowledge to help more accurate 3D detection, due to the fine-grained voxel-level semantic information can offer enhanced global perception capabilities. Certainly, the incorporation of instance-level discrimination within object detection can significantly enhance the distinctiveness of occupied voxels associated with different semantic labels. Consequently, this augmentation contributes to bolstering the certainty and accuracy in voxel-level semantic classification. Hence, the construction of a shared three-dimensional occupancy descriptor is proposed in [14, 20], enabling the unified execution of 3D object detection and occupancy prediction tasks.

However, the procession of three-dimensional voxel-level representations inevitably introduces complex computations, such as 3D (deformable) convolutions, transformer operators, and so on [13–15, 17, 20, 27]. This poses significant challenges for on-chip deployment and computational power requirements. Sparse occupancy representation is investigated in [22] to conserve memory resources. However, this approach does not fundamentally address the challenges for deployment and computation.

Noting the recent advancements in the utilization of FlashOcc [26] for BEVDetOcc [1], wherein all 3D convolutions are replaced with their 2D counterparts and a channel-to-height plugin is introduced. We observe that the main components of both BEVDet and FO(BEVDetOcc) remain consistent, the only differing components are the occupancy prediction head in FO(BEVDetOcc) and the detection head in BEVDet. This observation serves as a motivation to marry the occupancy prediction head to BEV neck of 3D object detection model, termed as UltimateDO. Consequently, our proposed UltimateDO successfully accomplishes the simultaneous execution of occupancy and detection tasks, while facilitating mutual enhancement between them. Extensive experiments reveals that the UltimateDO framework attains state-of-the-art (SOTA) performance with negligible additional time-consuming of only 1.1ms for the grafted occupancy prediction head. Additionally, our framework demonstrates superior performance on the nuScenes dataset.

2. Related Work

Image-based 3D Object Detection. Image-based 3D object detection has become a crucial element within autonomous driving perception systems, owing to its cost-effectiveness. It garners significant interest from both academia and industry. Previous approaches predominantly employed the paradigm of monocular 3D obstacle detection to perceive targets in the image perspective space. Subse-

quently, the perception results from multiple surround-view cameras were fused during the post-processing stage. Recently, there has been a notable shift towards employing the Lift-Splat-Shoot (LSS) technique to project surround-view image features onto the Bird’s Eye View (BEV) space for subsequent object detection in the BEV domain [7, 9]. Concurrently, the DETR-like paradigm has also gained significant attention and exploration. Specifically, it can be further classified into two categories: 3D-to-2D [12, 16, 21] and 2D-to-3D approaches [11, 23]. However, the results of obstacle detection are presented as coarse-grained rectangular bounding boxes (missing fine-grained details of object structures). Additionally, directly classifying unseen objects as background is not conducive to downstream planning tasks. Thus, occupancy prediction is proposed to address the above limitations.

3D Occupancy Prediction. The earliest origins of 3D occupancy prediction can be traced back to Occupancy Grid Maps (OGM) [19], which aimed to extract detailed structural information of the 3D scene from images, and facilitating downstream planning and navigation tasks. The existing studies can be classified into sparse perception and dense perception based on the type of supervision. The sparse perception category obtains direct supervision from lidar point clouds and are evaluated on lidar datasets [8]. Simultaneously, dense perception shares similarities with semantic scene completion (SSC) [2, 5]. Voxformer [10] utilizes 2.5D information to generate candidate queries and then obtains all voxel features via interpolation. Occ3D [20] reformulate a coarse-to-fine voxel encoder to construct occupancy representation. RenderOcc [14] extract 3D volume feature from surround views via 2D-to-3D network and predict density and label for each voxel with nerf Supervision. Furthermore, several benchmarks with dense occupancy labels are proposed [17, 20]. However, the above methods based on 3D voxel-level representation consumes huge computation, FlashOcc [26] utilizes the channel-to-height to perform the occupancy prediction on flattened BEV-level representation, with superior performance while least consumption.

Occupancy Interacted with Detection. A comprehensive understanding of 3D scene is beneficial for promoting the performance of the entire perception pipeline. Fine-grained structured information in occupancy representation facilitates 3D detection, [15] introduces occupancy attention learning for more accurate detection, [13] perform 3D detection via initialized from an binary occupancy pre-trained model. However, the above methods cannot achieve detection and occupancy simultaneously. Existing methods [17, 22] aim to integrate detection and segmentation into a unified learning framework, enabling dense scene semantics understanding with object-level instance discrimination, thus occupancy and detection can benefit each other under the joint-training framework. [17] constructs shared

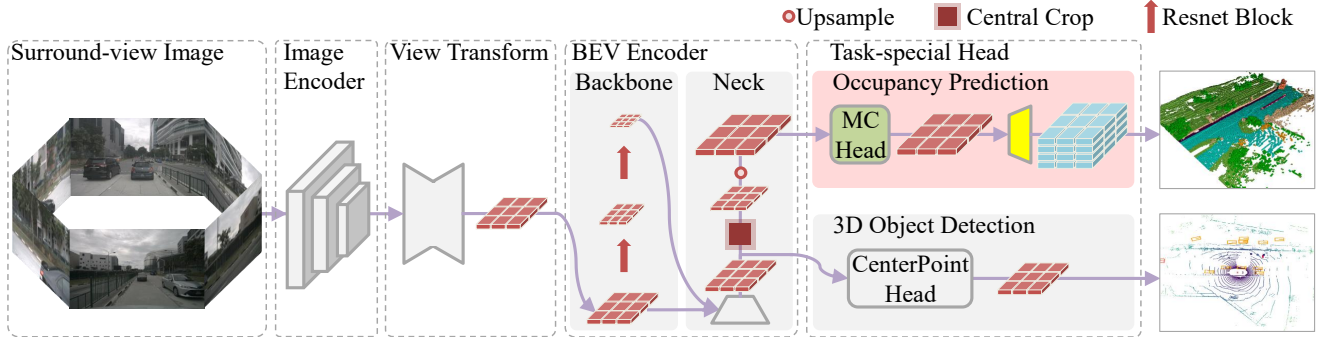


Figure 2. The diagram illustrates the overarching architecture of our proposed UltimateDO, which is best viewed in color and with zoom functionality. The region designated by the dashed box indicates the presence of replaceable modules. The light blue region corresponds to the optional temporal fusion module, and its utilization is contingent upon the activation of the red switch. MC is short for multi-convolution. Moreover, apart from the instructions provided for the three special icons located in the upper right corner, all remaining icons comply with the guidelines presented in Figure 1.

occupancy descriptor in a cascade fashion where voxels are refined progressively, which is then directly fed into occupancy and detection. [22] takes a step further to explore the sparse representation of occupancy to boost memory efficiency. The 3D voxel-level representation in these methods necessitates 3D computations, which inevitably leads to increased memory requirements and higher hardware deployment demands compared to purely 2D convolution models.

3. Framework

As illustrated in Figure. 2, the UltimateDO framework takes surround-view images as input and produces multiple outputs, including the forecasted 3D object bounding box with velocity information and dense occupancy prediction results.

Specifically, the surrounding-view images are fed into a 2D image encoder to extract high-level features in the perception-view. These features then undergo view transformation to obtain flattened BEV representations. The above coarse BEV information is further refined by passing through the BEV encoder, resulting in enhanced BEV features. The refined BEV features are utilized by task-specific heads for downstream perception tasks.

Indeed, considering that the perception range may vary between 3D object detection and occupancy prediction, as explicitly described in the training details of the experiment section, a central crop module is introduced to adjust the size of the BEV features specifically for the occupancy prediction branch, and an upsampling operator is employed to adjust the feature size to match the ground truth occupancy in the BEV dimension. This ensures that the occupancy prediction accurately corresponds to the desired perception range.

4. Experiment

In this section, we first detail the benchmark and metrics, as well as the training details for our framework in Section. 4.1. Then, Section. 4.2 presents the main results of our framework with fair comparison to other state-of-the-art methods on 3D object detection and occupancy prediction. After that, we conduct extensive ablative experiments to investigate the effectiveness of each component in our proposed framework in Section. 4.3.

4.1. Experimental Setup

Benchmark. We conducted occupancy and 3D object detection using the Occ3D-nuScenes [20] and nuScenes datasets [3], respectively. The Occ3D-nuScenes dataset comprises 700 scenes for training and 150 scenes for validation. The dataset covers a spatial range of -40m to 40m along the X and Y axes, and -1m to 5.4m along the Z axis. The occupancy labels are defined using voxels with dimensions of $0.4m \times 0.4m \times 0.4m$ for 17 categories. The nuScenes dataset consists of 1,000 distinct driving scenes, which are divided into three subsets: 700 training scenes, 150 validation scenes, and 150 testing scenes. Each driving scene contains 20 seconds of annotated perceptual data captured at a frequency of 2 Hz. The dataset encompasses 16 categories, including 6 background stuff categories and 10 foreground thing categories. The data collection vehicle is equipped with one LiDAR, five radars, and six cameras, enabling a comprehensive surround view of the vehicle’s environment.

Evaluation metrics. For occupancy prediction, the mean intersection-over-union (mIoU) over all classes is reported. For 3D object detection, we follow the official protocol to report the nuScene Score (NDS), mean Average

Table 1. 3D occupancy prediction performance on the Occ3D-nuScenes valuation dataset. * denotes initialized from the pre-trained FCOS3D backbone. Cons. Veh represents construction vehicle and Dri. Sur is for driveable surface. The frame per second (FPS) metric is evaluated using RTX3090, employing the TensorRT benchmark with FP16 precision. And the FPS is tested for the total model including occupancy and detection head.

Method	Backbone	Image size	mIoU \uparrow	FPS \uparrow	others \uparrow	barrier \uparrow	bicycle \uparrow	bus \uparrow	car \uparrow	Cons. Veh \uparrow	motorcycle \uparrow	pedestrian \uparrow	traffic cone \uparrow	trailer \uparrow	truck \uparrow	Dri. Sur \uparrow	other flat \uparrow	sidewalk \uparrow	terrain \uparrow	manmade \uparrow	vegetation \uparrow
BEVDetOcc [1]	R101*	512 \times 1408	32.81	27.3	7.61	38.28	9.62	39.68	46.57	17.99	14.88	18.10	10.38	30.08	33.14	80.04	38.00	49.51	52.37	38.21	33.25
FlashOcc [26]	R101*	512 \times 1408	33.4	29.6	7.54	39.14	11.37	40.93	47.06	14.52	14.82	16.57	11.27	30.83	33.65	80.77	41.04	49.93	53.75	40.01	34.22
UltimateDO	R101*	512 \times 1408	35.1	27.0	6.24	43.75	19.67	42.69	50.68	15.04	22.16	21.3	20.7	30.74	36.69	79.79	38.41	48.16	51.71	37.87	31.75

Table 2. Comparison of different paradigms on the nuScenes val set. * initialized from a FCOS3D backbone. § with Class-balanced Grouping and Sampling (CBGS).

Methods	Backbone	Image Size	mAP \uparrow	NDS \uparrow	FPS \uparrow	mATE \downarrow	mASE \downarrow	mAOE \downarrow	mAVE \downarrow	mAAE \downarrow
DETR3D§ [?]	R101*	900 \times 1600	30.3	37.4	-	86.0	27.8	43.7	96.7	23.5
PGD§ [18]	R101*	900 \times 1600	33.5	40.9	-	73.2	26.3	42.3	1.28	17.2
BEVDet§ [7]	R101*	384 \times 1056	31.7	38.9	-	70.4	27.3	53.1	94.0	25.0
BEVDet§ [7]	SwinT	512 \times 1408	34.9	41.7	-	63.7	26.9	49.0	91.4	26.8
PETR§ [25]	R101	512 \times 1408	35.7	42.1	-	71.0	27.0	49.0	88.5	22.4
PETR§ [25]	R101*	512 \times 1408	36.6	44.1	-	71.7	26.7	41.2	83.4	19.0
PETR§ [25]	SwinT	512 \times 1408	36.1	43.1	-	73.2	27.3	49.7	80.8	18.5
UltimateDO	R101*	512 \times 1408	36.6	43.6	27.0	68.0	27.9	54.4	75.4	21.2

Precision (mAP), along with five true positive metrics including mean Average Translation Error (mATE), mean Average Scale Error (mASE), mean Average Orientation Error (mAOE), mean Average Velocity Error (mAVE) and mean Average Attribute Error (mAAE).

Training Details. For comprehensive comparison, we have conducted experiments with ResNet-50 and ResNet-101 as the backbone networks in our experiments. The architecture of the detection branch is mainly following the setting in BEVDet [7], wherein the scope extent of nuScenes dataset is [-51.2m, -51.2m, -5m, 51.2m, 51.2m, 3m]. The occupancy prediction head refers from FlashOcc [26], and the scope extent of Occ3D-nuScenes is [-40m, -40m, -1m, 40m, 40m, 5.4m]. Given that occupancy prediction and 3D object detection are jointly trained in our framework, to encompass the range of the aforementioned two benchmarks, the scope range is defined as -51.2m to 51.2m in x/y dimension and -5m to 5.4m in height dimension. The full-size BEV feature is forwarded to 3D object branch, whereas the center-cropped $100/128 * S_{BEV} \times 100/128 * S_{BEV}$ BEV feature is sent to occupancy branch, the S_{BEV} is set to 128 in our experiments. Unless otherwise stated, adamW optimizer with gradient clip is utilized, the learning rate is set to $2e-4$. The loss weight for cross-entropy loss in occupancy prediction λ_{Occ} is set to 5.0 defaultly. Only flip augmentation is utilized for BEV augmentation, while scale and rotate augmentations

are not employed. All experiments with a total batch size of 16 are trained for 24 epochs on 4 NVIDIA RTX3090 GPUs. Note that CBGS is not used for all experiments, and test augmentation methods are not utilized during the inference.

4.2. Comparison with State-of-the-art Methods

We compared the performance of our framework with other state-of-the-art methods on occupancy and 3D detection respectively.

In terms of occupancy prediction, we directly compare our framework with popular existing approaches, i.e. MonoScene [4], TPVFormer [8], OccFormer [27], CTF-Occ [20] and RenderOCC [14]. Besides, we also extend the main-stream BEVFormer [11] to occupancy prediction following setting in CTF-Occ [20]. As listed in Table. 1, 3D occupancy prediction performances on the Occ3D-nuScenes valuation dataset are listed. The results with ResNet-101 as backbone and 512×1408 as input size is evaluated, Our UltimateDO achieve 35.1 mIoU with 27.0 FPS. Note that the FPS is tested with the hole model including both detection and occupancy head.

In terms of 3D object detection, our UltimateDO, implemented without CBGS and without scale/rotate-augmentation for BEV feature, demonstrates substantial improvements in performance compared to competitors who utilize the CBGS strategy for data balance and employ scale/rotate-augmentation for robust BEV feature. Specif-

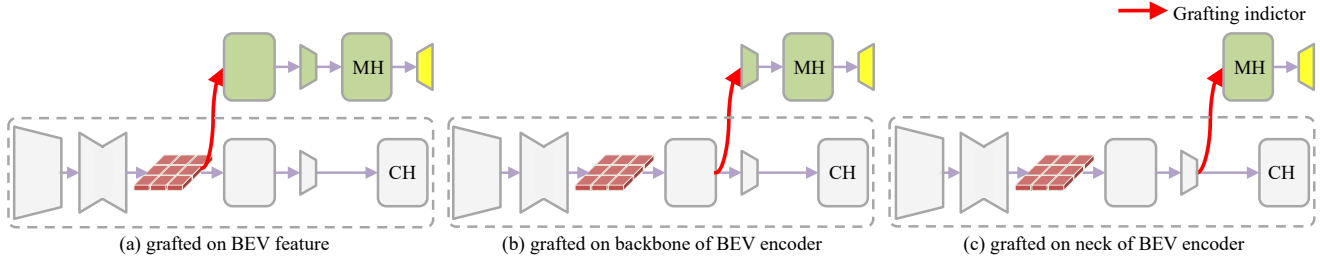


Figure 3. Illustration of occupancy branch grafted on (a) BEV feature; (b) backbone of BEV encoder; (c) neck of BEV encoder. The abbreviation "MH" represents MLP head, and "CH" stands for CenterPoint head. Icon interpretation descriptions follows Figure. 1. With the exception of the red line indicating the grafting location for occupancy branch, all other icons strictly adhere to the instructions depicted in Figure 1.

ically, our UltimateDO outperforms the origin BEVDet model with SwinT as the backbone by a margin of 1.7 mAP and 1.9 NDS. Additionally, when compared to the PETR model with SwinT as the backbone, our UltimateDO demonstrates superior performance with an improvement of 0.5 mAP and 0.5 NDS. Even when a enhanced ResNet-101 backbone, initialized from the pre-trained FCOS3D backbone, is employed for PETR, our UltimateDO maintains the same mAP performance and only suffers a marginal decrease of 0.5 NDS. These results highlight the effectiveness of our proposed UltimateDO in achieving competitive performance in 3D object detection tasks.

4.3. Ablation Study

We conduct ablative experiments to investigate the effect of each component in our framework. All the experiments are performed without CBGS strategy. Unless stated otherwise, we employ ResNet-50 as the backbone network with a input image resolution of 704 x 256. The default configuration did not include the temporal fusion module.

Where to Graft Occupancy Branch. The grafting location of the occupancy branch at an appropriate juncture is of paramount importance, as it influences: (1) the overall computational time and (2) the intricate interdependence and entanglement between detection and occupancy branches. Figure. 3 illustrates three progressive grafting schemes from shallow to deep. As illustrated in Table. 6, consider the setting when the occupancy branch is grafting on BEV feature and neck of BEV encoder, both approaches demonstrate comparable performance. However, there is a notable increase in time consumption of 3.6ms. Upon further examination of the comparison between all rows in Table 6, it is evident that the highest performance is attained when the grafting location is on the backbone of the BEV encoder. In comparison to the second competitor, this configuration yields a notable improvement of 0.3 mIoU, 0.4 mAP, and 0.4 NDS across all metrics. It further demonstrates that appropriately joint training the detection and occupancy features helps to integrate knowledge from di-

verse scenes, consequently leading to a mutually enhancing performance. However, the time-consumption is still 3ms larger compared to the setting when the grafting location is at the neck of BEV encoder. In conclusion, for large-scale offline inference in cloud-based settings, to achieve optimal perceptual accuracy, the configuration of grafting at backbone of BEV encoder is recommended. However, for deployment on edge devices with limited computational resources, we suggest adopting the more cost-effective configuration wherein the occupancy branch is graft on the neck of BEV encoder.

Grafting Location	mIoU	mAP	NDS	Time
BEV feat.	32.3	29.9	36.7	13.2ms
Bac. of BEV enc.	32.5	30.3	37.2	12.6ms
Neck of BEV enc.	32.2	29.7	36.8	9.1ms

Table 3. Impaction of Grafting Locations. "Time" denotes the time-consumption tested on RTX3090 by tensorrt with fp16 precision. "Bac." and "enc." short for backbone and encoder respectively.

Facilitation from Joint Training. As observation in last graph that sharing the modules before the neck of BEV encoder (Figure. 3 c) can facilitate mutual improvement of occupancy prediction and 3D object detection, with the optimal trade-off between precision and time-consumption. We conducted further ablation experiments to demonstrate the improvement achieved by joint training compared to separate training. As listed in Table. 6, joint training resulted in an improvement of 2.3 mIoU, 1.8 NDS and 1.4 mAP over independent trained occupancy or 3D object detection task, and only 1.1ms is consumed when occupancy branch is introduced to the detection module. The results demonstrate that fine-grained occupancy knowledge contributes to the construction of 3D semantic understanding within the model. Simultaneously, instance-level 3D bounding boxes aid in regulating the foreground space where objects are present. This reciprocal relationship between occupancy

prediction and 3D object detection highlights their potential to mutually facilitate each other in enhancing overall performance.

Occ.	Det.	mIoU	NDS	mAP	Time
✓		29.9	-	-	8.2ms
	✓	-	35.0	28.3	8.0ms
✓	✓	32.2 ^{+2.3}	36.8 ^{+1.8}	29.7 ^{+1.4}	9.1ms

Table 4. The improvement achieved by joint training compared to separate training. "Time" denotes the time-consumption tested on RTX3090 by tensorrt with fp16 precision. "OCC." denotes occupancy task, "Det." indicates 3D object detection.

Impact of Loss Weight λ_{Occ} for Joint Training. Due to feature coupling, different tasks in multi-task training may interfere with each other. It is common practice to use weight coefficients to adjust the importance of different tasks. We maintain the original detection loss weight to be 1.0, and experiment with different occupancy loss weight λ_{Occ} , specifically setting λ_{Occ} to 1.0, 5.0 and 8.0 respectively. The outcomes are presented in Table 5. It is evident that as the value of λ_{Occ} increases, there is a noticeable decline in mIoU, whereas mAP and NDS exhibit a tendency to rise. For a compromise balance, the loss weight λ_{Occ} is set to 5.0.

λ_{Occ}	mIoU	NDS	mAP
1.0	29.5	36.7	30.4
5.0	32.2	36.9	29.7
8.0	32.7	34.9	28.3

Table 5. Impact of Loss Weight λ_{Occ} for Joint Training.

Training without pretraining

Det. Init.	Occ.	Det.	mIoU	NDS	mAP
	✓		29.9	-	-
		✓	-	35.0	28.3
✓	✓		32.0	-	-
	✓	✓	32.2	36.8	29.7

Table 6. Benefit from joint training compared to separate training with pretrained detection. "Det. Init." represents that the model is initialized from the weight pretrained on BEVDet (second row in current Table). "OCC." denotes occupancy task, "Det." indicates 3D object detection.

Influence of BEV Augmentations. In general, BEV Augmentations typically involve operations such as flip, rotation, and scaling. Previous studies have shown that flip

augmentation is beneficial for both occupancy and 3D object detection. However, scaling augmentation can introduce truncation errors, leading to a degradation in performance. For this reason, it is not utilized in the BEVDetOcc, RenderOcc, and FBOcc methods. Additionally, while rotation augmentation is employed in FBOcc, it is not used in BEVDetOcc and RenderOcc. Therefore, we aim to investigate the impact of rotation augmentation on joint training. According to the results presented in Table. 7, it is observed that rotation augmentation makes no difference on mIoU but leads to inferior NDS scores, which contradicts the notion that BEV augmentation improves 3D object detection performance. Consequently, we have decided to retain only the flip augmentation as the BEV augmentation method for our joint training approach.

BEVAug	mIoU	NDS	mAP
Flip	32.2	36.9	29.7
Flip+Rotation	32.1	36.2	30.0

Table 7. Influence of BEV Augmentation.

5. Conclusion

To efficiently achieve occupancy prediction and 3D object detection, we marry the occupancy prediction head in FlashOcc to the BEV neck of BEVDet, resulting in a unified framework called UltimateDO. This integration allows UltimateDO to be easily deployed on various computing chips while maintaining high precision with minimal time consumption. Notably, UltimateDO does not rely on 3D convolution or transformer modules, and the occupancy prediction branch and detection branch can mutually benefit each other. Besides, merely 1.1ms computation for the grafted occupancy head. We believe that UltimateDO can serve as a robust baseline for the research community, and we are committed to expanding its application to other perception pipelines in autonomous driving systems.

References

- [1] <https://github.com/huangjunjie2017/bevdet>.
- [2] Iro Armeni, Sasha Sax, Amir R Zamir, and Silvio Savarese. Joint 2d-3d-semantic data for indoor scene understanding. *arXiv preprint arXiv:1702.01105*, 2017.
- [3] Holger Caesar, Varun Bankiti, Alex H Lang, Sourabh Vora, Venice Erin Liong, Qiang Xu, Anush Krishnan, Yu Pan, Giancarlo Baldan, and Oscar Beijbom. nuscenes: A multi-modal dataset for autonomous driving. In *Proceedings of the IEEE/CVF conference on computer vision and pattern recognition*, pages 11621–11631, 2020.
- [4] Anh-Quan Cao and Raoul de Charette. Monoscene: Monocular 3d semantic scene completion. In *Proceedings of the IEEE/CVF Conference on Computer Vision and Pattern Recognition*, pages 3991–4001, 2022.

- [5] Angela Dai, Angel X Chang, Manolis Savva, Maciej Halber, Thomas Funkhouser, and Matthias Nießner. Scannet: Richly-annotated 3d reconstructions of indoor scenes. In *Proceedings of the IEEE conference on computer vision and pattern recognition*, pages 5828–5839, 2017.
- [6] Yihan Hu, Jiazhi Yang, Li Chen, Keyu Li, Chonghao Sima, Xizhou Zhu, Siqi Chai, Senyao Du, Tianwei Lin, Wenhai Wang, Lewei Lu, Xiaosong Jia, Qiang Liu, Jifeng Dai, Yu Qiao, and Hongyang Li. Planning-oriented autonomous driving. In *Proceedings of the IEEE/CVF Conference on Computer Vision and Pattern Recognition*, 2023.
- [7] Junjie Huang, Guan Huang, Zheng Zhu, Yun Ye, and Dalong Du. Bevdet: High-performance multi-camera 3d object detection in bird-eye-view. *arXiv preprint arXiv:2112.11790*, 2021.
- [8] Yuanhui Huang, Wenzhao Zheng, Yunpeng Zhang, Jie Zhou, and Jiwen Lu. Tri-perspective view for vision-based 3d semantic occupancy prediction. *arXiv preprint arXiv:2302.07817*, 2023.
- [9] Yinhao Li, Zheng Ge, Guanyi Yu, Jinrong Yang, Zengran Wang, Yukang Shi, Jianjian Sun, and Zeming Li. Bevddepth: Acquisition of reliable depth for multi-view 3d object detection. *arXiv preprint arXiv:2206.10092*, 2022.
- [10] Yiming Li, Zhiding Yu, Christopher Choy, Chaowei Xiao, Jose M Alvarez, Sanja Fidler, Chen Feng, and Anima Anandkumar. Voxformer: Sparse voxel transformer for camera-based 3d semantic scene completion. In *Proceedings of the IEEE/CVF Conference on Computer Vision and Pattern Recognition*, pages 9087–9098, 2023.
- [11] Zhiqi Li, Wenhai Wang, Hongyang Li, Enze Xie, Chonghao Sima, Tong Lu, Qiao Yu, and Jifeng Dai. Bevformer: Learning bird’s-eye-view representation from multi-camera images via spatiotemporal transformers. *arXiv preprint arXiv:2203.17270*, 2022.
- [12] Yingfei Liu, Tiancai Wang, Xiangyu Zhang, and Jian Sun. Petr: Position embedding transformation for multi-view 3d object detection. *arXiv preprint arXiv:2203.05625*, 2022.
- [13] Chen Min, Liang Xiao, Dawei Zhao, Yiming Nie, , and Bin Dai. Multi-camera unified pre-training via 3d scene reconstruction. *arXiv preprint*, 2023.
- [14] Mingjie Pan, Jiaming Liu, Renrui Zhang, Peixiang Huang, Xiaoqi Li, Li Liu, and Shanghang Zhang. Renderocc: Vision-centric 3d occupancy prediction with 2d rendering supervision. *arXiv preprint arXiv:2309.09502*, 2023.
- [15] Liang Peng, Junkai Xu, Haoran Cheng, Zheng Yang, Xiaopei Wu, Wei Qian, Wenxiao Wang, Boxi Wu, and Deng Cai. Learning occupancy for monocular 3d object detection. *arXiv preprint*, 2023.
- [16] Changyong Shu, Jiajun Deng, Fisher Yu, and Yifan Liu. 3dppe: 3d point positional encoding for multi-camera 3d object detection transformers. *arXiv preprint arXiv:2211.14710*, 2023.
- [17] Chonghao Sima, Wenwen Tong, Tai Wang, Li Chen, Silei Wu, Hanming Deng, Yi Gu, Lewei Lu, Ping Luo, Dahua Lin, and Hongyang Li. Scene as occupancy. 2023.
- [18] Wang Tai, Zhu Xinge, Pang Jiangmiao, and Lin Dahua. Probabilistic and Geometric Depth: Detecting objects in perspective. In *Conference on Robot Learning (CoRL) 2021*, 2021.
- [19] Sebastian Thrun. Probabilistic robotics. *Communications of the ACM*, 45(3):52–57, 2002.
- [20] Xiaoyu Tian, Tao Jiang, Longfei Yun, Yue Wang, Yilun Wang, and Hang Zhao. Occ3d: A large-scale 3d occupancy prediction benchmark for autonomous driving. *arXiv preprint arXiv:2304.14365*, 2023.
- [21] Shihao Wang, Yingfei Liu, Tiancai Wang, Ying Li, and Xiangyu Zhang. Exploring object-centric temporal modeling for efficient multi-view 3d object detection. *arXiv preprint arXiv:2303.11926*, 2023.
- [22] Yuqi Wang, Yuntao Chen, Xingyu Liao, Lue Fan, and Zhaoxiang Zhang. Panoocc: Unified occupancy representation for camera-based 3d panoptic segmentation. *arXiv preprint arXiv:2306.10013*, 2023.
- [23] Yue Wang, Vitor Campagnolo Guizilini, Tianyuan Zhang, Yilun Wang, Hang Zhao, and Justin Solomon. Detr3d: 3d object detection from multi-view images via 3d-to-2d queries. In *Conference on Robot Learning*, pages 180–191. PMLR, 2022.
- [24] Liu Yingfei, Yan Junjie, Jia Fan, Li Shuailin, Gao Qi, Wang Tiancai, Zhang Xiangyu, and Sun Jian. PetrV2: A unified framework for 3d perception from multi-camera images. *arXiv preprint arXiv:2206.01256*, 2022.
- [25] Liu Yingfei, Wang Tiancai, Zhang Xiangyu, and Sun Jian. Petr: Position embedding transformation for multi-view 3d object detection. *arXiv preprint arXiv:2203.05625*, 2022.
- [26] Zichen Yu, Changyong Shu, Jiajun Deng, Kangjie Lu, Zongdai Liu, Jiangyong Yu, Dawei Yang, Hui Li, and Yan Chen. Flashocc: Fast and memory-efficient occupancy prediction via channel-to-height plugin. *arXiv preprint arXiv:2311.12058*, 2023.
- [27] Yunpeng Zhang, Zheng Zhu, and Dalong Du. Occformer: Dual-path transformer for vision-based 3d semantic occupancy prediction. *arXiv preprint arXiv:2304.05316*, 2023.
- [28] Li Zhiqi, Wang Wenhai, Li Hongyang, Xie Enze, Sima Chonghao, Lu Tong, Yu Qiao, and Dai Jifeng. Bevformer: Learning bird’s-eye-view representation from multi-camera images via spatiotemporal transformers. *arXiv preprint arXiv:2203.17270*, 2022.